Low-Noise Nano Superconducting Quantum Interference Device Operating in Tesla Magnetic Fields

Tobias Schwarz, Joachim Nagel, Roman Wölbing, Matthias Kemmler, Reinhold Kleiner, and Dieter Koelle*

Physikalisches Institut—Experimentalphysik II and Center for Collective Quantum Phenomena in LISA$^+$, Universität Tübingen, Auf der Morgenstelle 14, D-72076 Tübingen, Germany

ABSTRACT Superconductivity in the cuprate $YBa_2Cu_3O_7$ (YBCO) persists up to huge magnetic fields (B) up to several tens of Teslas, and sensitive direct current (dc) superconducting quantum interference devices (SQUIDs) can be realized in epitaxially grown YBCO films by using grain boundary Josephson junctions (GBJs). Here we present the realization of high-quality YBCO nanoSQUIDs, patterned by focused ion beam milling. We demonstrate low-noise performance of such a SQUID up to $B = 1$ T applied parallel to the plane of the SQUID loop at the temperature $T = 4.2$ K. The GBJs are shunted by a thin Au layer to provide nonhysteretic current voltage characteristics, and the SQUID incorporates a 90 nm wide constriction which is used for on-chip modulation of the magnetic flux through the SQUID loop. The white flux noise of the device increases only slightly from 1.3 $\mu\Phi_0/(\mathrm{Hz})^{1/2}$ at $B = 0$ to 2.3 $\mu\Phi_0/(\mathrm{Hz})^{1/2}$ at 1 T. Assuming that a point-like magnetic particle with magnetization in the plane of the SQUID loop is placed directly on top of the constriction and taking into account the geometry of the SQUID, we calculate a spin sensitivity $S_\mu^{1/2} = 62\ \mu_B/(\mathrm{Hz})^{1/2}$ at $B = 0$ and 110 $\mu_B/(\mathrm{Hz})^{1/2}$ at 1 T. The demonstration of low noise of such a SQUID in Tesla fields is a decisive step toward utilizing the full potential of ultrasensitive nanoSQUIDs for direct measurements of magnetic hysteresis curves of magnetic nanoparticles and molecular magnets.

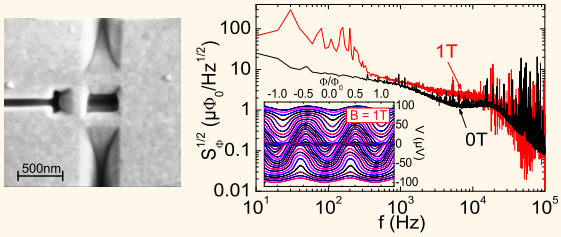

KEYWORDS: YBCO · SQUID · superconductivity · nanofabrication · flux noise · spin sensitivity · magnetic particle detection

Growing interest in the detection and investigation of small spin systems like single-molecular/single-chain magnets,[1,2] cold atom clouds,[3] or even single electrons/atoms[4] demands for sensors that are sensitive to very small changes of the magnetization of small particles with the ultimate goal of single spin detection. The interest for the investigation of such particles affects many fields of research such as material science, chemistry, information technology, medical and biological science, or studies of quantum effects in mesoscopic matter. In order to meet the challenge of detecting a single electron spin, various techniques such as magnetic resonance force microscopy,[5] magneto-optic spin detection,[6,7] and scanning tunneling microscopy assisted electron spin resonance[8,9] have been adapted.

In contrast to these techniques, miniaturized Hall bars[10,11] or direct current (dc) superconducting quantum interference devices (SQUIDs)[12−29] offer the possibility of measuring directly magnetization changes in small spin systems by probing changes of the particle's stray magnetic field or magnetic flux coupled to the Hall bars or SQUIDs, respectively. Such devices can be operated continuously as field-to-voltage or flux-to-voltage converters (for dc SQUIDs with nonhysteretic Josephson junctions), allowing one to investigate magnetization dynamics of the sample under investigation. Indeed, apart from pioneering work by Wernsdorfer *et al.* using microSQUIDs for the measurements of the magnetization of nanoparticles,[13] recent publications reported on preliminary measurements of small clusters of nanoparticles by using nanoSQUIDs with a flux capture area below 1 μm^2.[22,26,30]

For SQUIDs, scaling down their size to the submicrometer range offers the possibility to reach extremely low values of the spectral density of flux noise power S_Φ (*via* reduction of the inductance L of the SQUID loop).[31] Furthermore, by placing a magnetic particle on top of a very narrow constriction intersecting the SQUID loop, one can achieve a large coupling factor $\phi_\mu \equiv \Phi/\mu$, that is, the amount of magnetic flux Φ

* Address correspondence to koelle@uni-tuebingen.de.

Received for review November 22, 2012 and accepted December 19, 2012.

Published online December 19, 2012
10.1021/nn305431c

which is coupled by a particle with magnetic moment μ to the SQUID loop. Hence, it has been proposed that nanoSQUIDs may reach spin sensitivities $S_\mu^{1/2} \equiv S_\Phi^{1/2}/\phi_\mu$ of only a few $\mu_B/(\mathrm{Hz})^{1/2}$,[32] where μ_B is the Bohr magneton. Taking $\phi_\mu \approx 20\ n\Phi_0/\mu_B$, for example, which is achievable as we demonstrate below, a spin sensitivity of 1 $\mu_B/(\mathrm{Hz})^{1/2}$ requires an ultralow rms flux noise $S_\Phi^{1/2} = 20\ n\Phi_0/(\mathrm{Hz})^{1/2}$ (Φ_0 is the magnetic flux quantum). We note that state-of-the art, nonminiaturized dc SQUIDs reach values for $S_\Phi^{1/2}$ on the order of 1 $\mu\Phi_0/(\mathrm{Hz})^{1/2}$.[33] However, for very low inductance SQUIDs, values of $S_\Phi^{1/2}$ down to $\sim$20 $n\Phi_0/(\mathrm{Hz})^{1/2}$ have been demonstrated indeed.[31]

So why have we not seen demonstrations of measurements of magnetization reversals of small magnetic particles by using ultrasensitive dc nanoSQUIDs so far? The reason for this is that such measurements typically require the application of very strong magnetic fields in the Tesla range,[13] while very low flux noise in SQUIDs has been demonstrated only for operation of such SQUIDs in the earth's magnetic field ($\sim$60 μT) or, more typically, in a magnetically well-shielded environment in the nT range (*i.e.*, 9 orders of magnitude lower magnetic fields).[33]

Miniaturized nanoSQUIDs based on very thin Nb films with constriction-type Josephson junctions have been operated in impressive background fields in the Tesla range.[34,27] Chen *et al.*[34] achieved operation in fields up to 7 T for SQUIDs made of $d \sim 5.5$ nm thin Nb films. However, there are two drawbacks in this design. First, the very low thickness of the Nb film causes the (kinetic) SQUID inductance L ($\propto 1/d$) and consequently the SQUID flux noise power S_Φ ($\propto L$) to be large,[35] at least 4 orders of magnitude above the values obtained for sensitive state-of-the-art SQUIDs. Second, the constriction junctions have a hysteretic current voltage characteristic (IVC). This prevents continuous measurements and the use of advanced readout schemes,[36] which are required for ultrasensitive dc SQUIDs. Similar values for the flux noise (at $B \sim 0.3$ T) have been reported very recently for boron-doped diamond μ-SQUIDs based on constriction junctions, which operated up to 4 T.[29] For $B > 0.5$ T, the IVCs became nonhysteretic; however, noise data at such high fields have not been reported, and the very low transfer function $V_\Phi \equiv (\partial V/\partial\Phi)_{max} \approx 0.5\ \mu V/\Phi_0$ at $B = 1$ T implies probably similar noise performance as for lower fields (V is the voltage across the SQUID).

We should note here that very sensitive Nb thin film (d = 200 nm) nanoSQUIDs based on nonhysteretic constriction type junctions, resistively shunted with a 150 nm thick W layer, have been realized with $S_\Phi^{1/2} = 0.2\ \mu\Phi_0/(\mathrm{Hz})^{1/2}$.[37] However, these devices are probably only suited for operation in subTesla fields[38] and show optimum performance only in a narrow temperature range not too far below the transition temperature (T_c) of Nb. This makes them less interesting for applications which are most promising for temperatures of a few Kelvin and well below.[13]

In order to fully exploit the potential of SQUIDs, there is thus a clear need to develop sensitive nanoSQUIDs with nonhysteretic IVCs that at the same time can be operated in strong background fields. As for the SQUIDs with constriction junctions, such SQUIDs should incorporate at least one very thin and/or narrow section where the magnetic particle is placed, allowing for a good coupling of the magnetic stray field of the particle to the SQUID. This all calls for a superconductor which has a very high critical field and allows for patterning nanosized structures and not too large Josephson junctions. The cuprate superconductor $YBa_2Cu_3O_7$ (YBCO) fulfills these requirements. Compared to Nb, YBCO is not a mature material and even the most reliable type of YBCO Josephson junctions, such as grain boundary junctions (GBJs), exhibit a large $1/f$ noise as well as an appreciable scatter in their electrical parameters.[39,40] Nonetheless, based on a recently developed process for fabricating high-quality submicrometer YBCO grain boundary junctions,[41] SQUIDs with high spin sensitivity can be fabricated reproducibly. YBCO GBJ SQUIDs have already been demonstrated to operate in $B = 1$ T[4] and were used to measure magnetization curves of microscale magnets in fields up to 0.12 T,[42] however, with poor noise performance. Here, we show that this field scale can be extended to above 1 T, while still maintaining state-of-the art noise performance of the SQUID.

RESULTS AND DISCUSSION

Sample Fabrication and Layout. The YBCO nanoSQUIDs were made in a similar way, as described in Nagel *et al.*[41] Using pulsed laser deposition, epitaxial *c*-axis-oriented YBCO thin films of thickness $d = 50$ nm were grown on $SrTiO_3$ (STO) [001] bicrystal substrates with misorientation angle $\Theta = 24°$. Subsequently, a Au layer of thickness $d_{Au} = 60$ nm was evaporated *in situ*, serving as a shunt resistance for the YBCO GBJs (providing nonhysteretic IVCs at the envisaged operation temperature $T = 4.2$ K and below) and also acting as a protection layer during focused ion beam (FIB) milling. The critical temperature (T_c) of the YBCO film, measured inductively, was $\sim$91 K.

To obtain the nanoSQUID, structures with line widths down to 1 μm (at the region of the grain boundary) were prepatterned by photolithography and Ar ion milling. Subsequently, two nanoscaled Josephson junctions and a constriction next to the SQUID loop, which permits modulation of the SQUID by applying an additional current I_{mod}, were patterned by FIB. Cutting deep into the STO substrate results in sloped junction edges due to redeposition of amorphous YBCO and STO, which should help to prevent oxygen outdiffusion from the YBCO film. With this procedure, we could fabricate high-performance SQUIDs with junction

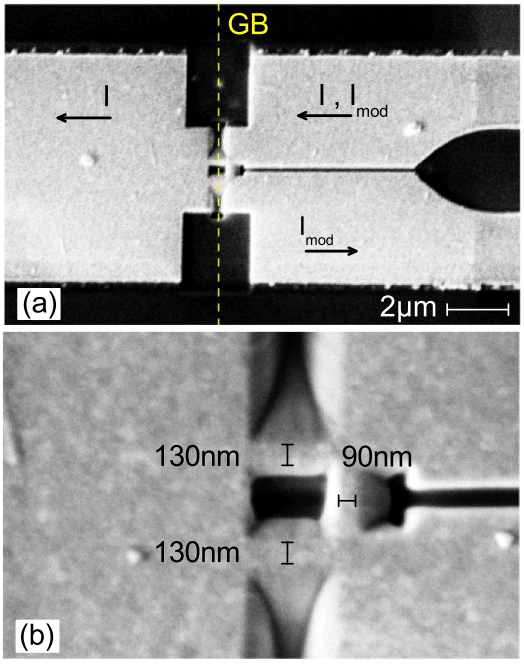

Figure 1. SEM images of the nanoSQUID. In (a), the directions of the modulation and bias currents I_{mod} and I are indicated by arrows, and the grain boundary (GB) is indicated by the vertical dashed line. In (b), the widths of the most narrow sections of the nanoSQUID are indicated.

widths w_J down to ~100 nm. The SQUIDs had almost identical transport and noise characteristics. Below, we discuss data of one device.

Figure 1 shows a scanning electron microscope (SEM) image of the nanoSQUID with a hole size of 300 nm × 400 nm. The junctions have a width $w_J \approx$ 130 nm, and the lengths of the bridges containing the junctions are $l_J \approx 400$ nm. The constriction has a width $w_c \approx 90$ nm and length $l_c = 300$ nm. A bias current I flowing across the junctions, as well as a modulation current I_{mod} flowing across the constriction are applied as indicated by arrows in Figure 1a.

Electric Transport Data. All measurements were performed at $T = 4.2$ K with the magnetic field B carefully aligned in the plane of the SQUID loop. Figure 2a shows the IVC of the nanoSQUID at $B = 0$ and $I_{mod} = 0$. We find a critical current of the SQUID $I_c = 2I_0 = 37\ \mu$A and a resistance $R/2 = 3.5\ \Omega$, which results in $I_0R = 130\ \mu$V (I_0 and R refer to the average junction critical current and resistance, respectively). The corresponding values $j_0 = I_0/(w_J d) = 2.85$ mA/μm^2, $\rho = Rw_J d = 0.046\ \Omega\cdot\mu$m^2, and the value for I_0R are close to the values obtained for earlier devices.[41] Very slightly above I_c, the voltage increases continuously from zero, but then the IVC develops a small hysteresis between 15 and 70 μV. This is presumably caused by some Fiske or LC-type resonance, which prevented accurately fitting the resistive part of this IVC to a resistively and capacitively shunted junction (RCSJ) model.[43,44] Simulations using Langevin equations[45] were still possible for $I_c(I_{mod})$.

Figure 2b shows the measured $I_c(I_{mod})$ at $B = 0$ (solid black line), together with $I_c(I_{mod})$ curves at $B = 1$ and 3 T, which will be discussed below. The data for $B = 0$ are fitted well by the Langevin simulations, which is shown as the dashed cyan line. For the simulations, we have used a noise parameter $\Gamma = 2\pi k_B T/I_0\Phi_0 = 0.01$, corresponding to the measured value of I_0 at $T = 4.2$ K. We further used an inductance asymmetry $\alpha_L = (L_2 - L_1)/(L_1 + L_2) = 0.175$ due to asymmetric biasing of the device; here, L_1 and L_2 are the inductance of the upper and lower arm of the SQUID, respectively (cf. Figure 1). We also used a junction critical current asymmetry $\alpha_i = (I_{02} - I_{01})/(I_{01} + I_{02}) = 0.22$. For the inductance parameter, the simulations yield $\beta_L \equiv 2I_0L/\Phi_0 = 0.65$, which results in $L = 36$ pH. From the $I_c(I_{mod})$ modulation period, we find for the magnetic flux Φ, coupled to the SQUID by I_{mod}, the value $\Phi/I_{mod} = 3.1\ \Phi_0$/mA, which corresponds to a mutual inductance $M_{mod} = 6.4$ pH. We note that the values quoted above for L and M_{mod} are determined experimentally; given the geometry of our device, these values seem to be consistent. However, using standard expressions taking into account the large contribution of the kinetic inductance due to the small YBCO film thickness $d \ll \lambda_L$ (λ_L is the London penetration depth), one expects much smaller values for L and M_{mod}. The reason for this is still unclear. The final parameter to be determined is the Stewart–McCumber parameter $\beta_C \equiv 2\pi I_0R^2C/\Phi_0$, where C is the junction capacitance. Since we cannot fit the experimental IVC accurately, we cannot infer a precise number here. However, due to the fact that a small hysteresis shows up in limited ranges of bias current and applied flux, we assume that β_C is on the order of 1, yielding $C \approx 0.36$ pF. Figure 2c shows the $V(\Phi)$ characteristics of the device for bias currents I ranging from −49.5 to 49.5 μA at $B = 0$. Near $I = I_c$, the curves are hysteretic. The transfer function, that is, the maximum slope of the $V(\Phi)$ curves at optimum I (determined for the nonhysteretic curves), is $V_\Phi = 500\ \mu V/\Phi_0$.

For further measurements, the nanoSQUID was shunted by the input circuit of the SQUID amplifier with an input resistance $R_{inp} = 10\ \Omega$. The additional shunt resistance reduces β_C, yielding nonhysteretic IVCs and $V(I_{mod})$ characteristics; in this case, $V_\Phi \approx 450\ \mu V/\Phi_0$ (at $B = 0$).

At $B = 1$ T (cf. dashed red line in Figure 2b), the $I_c(I_{mod})$ characteristics show a slightly suppressed maximum critical current $I_c(1\ T) = 30\ \mu$A. This pattern is shifted in comparison to the $B = 0$ data, as the SQUID is not perfectly aligned to the magnetic field and flux couples into the Josephson junctions and the SQUID loop. In addition, when sweeping I_{mod} back and forth, a hysteresis becomes visible in a small interval of I_{mod}, presumably caused by Abrikosov vortices trapped in the bias leads. Flux jumps caused by Abrikosov vortices also affect the modulation period, reducing it by about 5% in the interval plotted in Figure 2b. Figure 2d shows

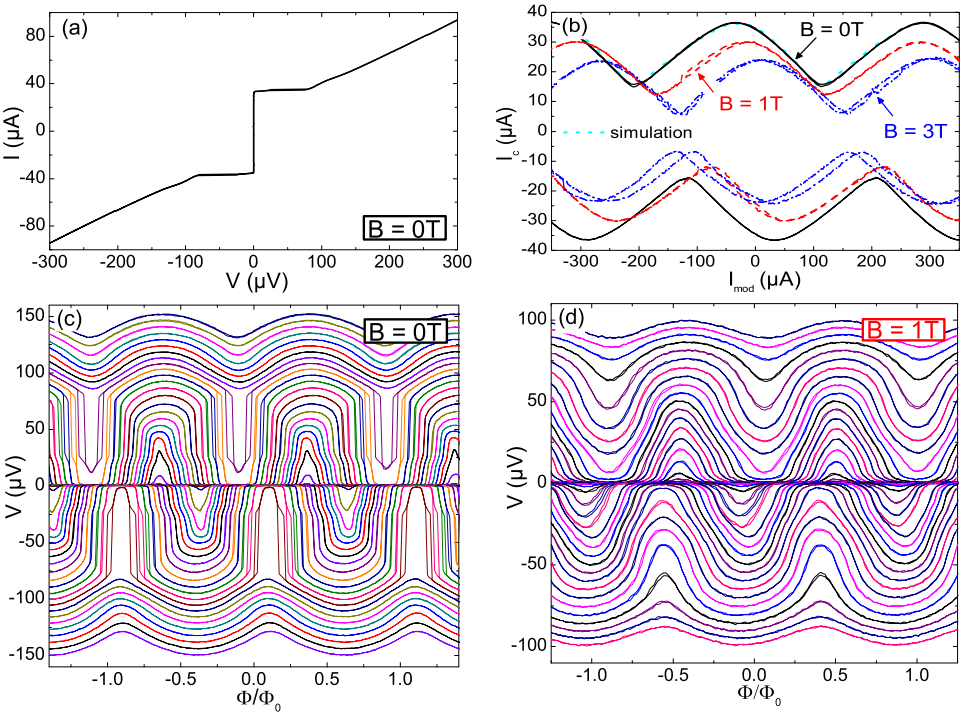

Figure 2. Transport characteristics of the nanoSQUID: (a) IVC at $I_{mod} = 0$ and $B = 0$. (b) Critical current $I_c(I_{mod})$ for $B = 0$, 1, and 3 T; for comparison, the numerically calculated curve for $B = 0$ is also shown. (c) $V(\Phi)$ at $B = 0$ for $I = -49.5 \ldots 49.5$ μA (in 1.5 μA steps.) (d) $V(\Phi)$ at $B = 1$ T for currents fed to the SQUID which is shunted by the input resistance $R_{inp} = 10\ \Omega$ of the SQUID amplifier $I_b = -40.5 \ldots 40.5$ μA (in 1.5 μA steps.) All curves in (a–d) were traced out in both sweep directions.

$V(\Phi)$ characteristics at $B = 1$ T for currents I_b (fed to the SQUID which is shunted by R_{inp}) ranging from -40.5 to 40.5 μA. The IVCs are nonhysteretic and hence the $V(\Phi)$ characteristics are smooth, exhibiting no jumps as in Figure 2c. The lack of hysteresis is either due to the additional shunt resistance R_{inp} or due to the strong magnetic field suppressing the critical current. The transfer function is $V_\Phi = 350\ \mu V/\Phi_0$. Interestingly, the hysteresis in $V(\Phi)$ at $B = 1$ T upon sweeping the applied flux in both directions almost disappeared, which is helpful for reading out the SQUID when operated in strong magnetic fields.

Upon increasing B up to 3 T, still periodic $I_c(I_{mod})$ characteristics with only a slightly suppressed maximum critical current $I_c = 24$ μA could be measured, as shown in Figure 2b as blue dashed-dotted lines. The shift in comparison to the $B = 0$ data did increase further, and also the hysteresis did increase, as mentioned above presumably due to vortices in the bias leads. These data clearly show that the SQUID is operating also in $B = 3$ T. As mentioned above, noise measurements could not be performed for fields much higher than 1 T since the SQUID amplifier trapped magnetic flux. However, this is just a technical problem which can be solved in future measurements by implementing field compensation *via* a coil mounted around the Nb shield.

Flux Noise Measurements. Figure 3 summarizes the flux noise spectra $S_\Phi^{1/2}(f)$ of the nanoSQUID at $B = 0$ and $B = 1$ T at the optimum working point.

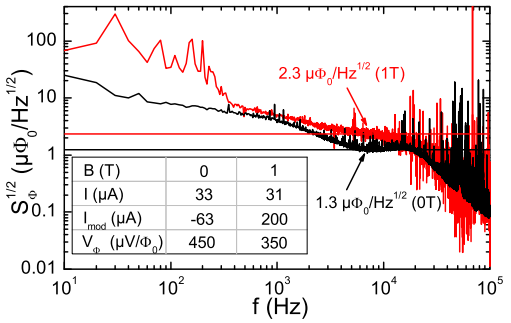

Figure 3. Flux noise spectra of the nanoSQUID at optimum working points at $B = 0$ and 1 T. The horizontal lines indicate the white noise levels.

As measurements were performed without magnetic shielding, noise spikes occur on both spectra. The noise data were corrected for the noise contribution of the amplifier. In both cases, $S_\Phi^{1/2}$ increases for frequencies f below ~3 kHz, a behavior which at least for $B = 0$ is known to arise from critical current fluctuations of the junctions. This contribution can, in principle, be eliminated by proper modulation techniques (bias reversal).[46] At $B = 1$ T, there are presumably additional contributions due to fluctuating Abrikosov vortices. Note, however, that between ~300 Hz and 3 kHz the noise level is less than a factor of 2 higher at $B = 1$ T as compared to $B = 0$. The decrease in $S_\Phi^{1/2}$ above 10 kHz is caused by the limited bandwidth of our measurement setup. At $B = 0$, the white noise level averaged between 6 and 7 kHz is 1.3 $\mu\Phi_0/(\text{Hz})^{1/2}$. For $B = 1$ T, we determine

a rms flux noise of 2.3 $\mu\Phi_0/(\mathrm{Hz})^{1/2}$ averaged between 6 and 7 kHz.

These numbers may be compared to the theoretical expression obtained from Langevin simulations, $S_\Phi = f(\beta_L)\Phi_0 k_B TL/I_0 R$, which is valid for $\beta_C \lesssim 1$.[47] For $\beta_L > 0.4$, $f(\beta_L) \approx 4(1 + \beta_L)$. For lower values of β_L, S_Φ increases. For the parameters of our device, we calculate $S_\Phi^{1/2} = 0.23\ \mu\Phi_0/(\mathrm{Hz})^{1/2}$, that is, a factor of almost 6 less than the experimental value at $B = 0$. Such an excess noise is not unusual for YBCO SQUIDs.[46]

Finally, we note that the observed increase by a factor of ~1.8 in $S_\Phi^{1/2}$ at 6−7 kHz upon increasing B from 0 to 1 T cannot be explained by the reduction of I_0 and V_Φ. From the above-mentioned expression for S_Φ, one would only expect an increase in the white rms flux noise by ~10%. However, we note that in the flux noise data for B = 1 T (cf. Figure 3) no clear white noise is observable. Hence, the quoted value for $S_\Phi^{1/2}(B = 1\ \mathrm{T})$ should be seen as an upper limit for the white noise level.

Spin Sensitivity. In order to estimate the spin sensitivity $S_\mu^{1/2} = S_\Phi^{1/2}/\phi_\mu$ of the nanoSQUID, we numerically calculated the coupling factor $\phi_\mu = \Phi/\mu$, that is, the flux Φ coupled into the SQUID loop by a point-like particle with magnetic moment μ, using the software package 3D-MLSI.[48] Details on the calculation procedure can be found in Nagel *et al.*[41] In brief, one calculates the magnetic field distribution $\vec{B}(\vec{r})$ generated by a current J circulating around the SQUID hole. The coupling factor is obtained from $\phi_\mu = -\hat{e}_\mu \vec{B}(\vec{r})/J$. Here, $\hat{e}_\mu$ is the direction of the magnetic moment $\vec{\mu}$ at position $\vec{r}$. The results of these calculations are summarized in Figure 4 for a point-like particle with magnetic moment pointing in the x-direction. The particle is located in the (x,z) plane (perpendicular to the plane of the SQUID loop in the (x,y) plane) at position $y = 0$ and $x = 0$ to 1000 nm, as indicated by the dashed line in the SEM image shown in Figure 4a. The contour plot in Figure 4b shows $\phi_\mu(x,z)$ for values of $z = 0$ (substrate surface) up to z = 1000 nm. Figure 4c shows a linescan $\phi_\mu(x)$ through this plane, as indicated by the horizontal dashed line in Figure 4b. The linescan is taken at a distance of 10 nm above the Au layer. The coupling factor ϕ_μ has a maximum of 9.2 $n\Phi_0/\mu_B$ at the position of the constriction at $x \approx 0.64\ \mu$m. The minimum in $\phi_\mu(x)$ is slightly left from the center of the SQUID loop; this is because the constriction breaks symmetry. Figure 4d shows a linescan taken along the vertical dashed line in graph (b). The coupling factor ϕ_μ decreases strongly with increasing z. Calculating the spin sensitivity with ϕ_μ = 9.2 $n\Phi_0/\mu_B$, we obtain $S_\mu^{1/2} = 141\ \mu_B/(\mathrm{Hz})^{1/2}$ at $B = 0$ and 250 $\mu_B/(\mathrm{Hz})^{1/2}$ at B = 1 T. In principle, the particle could be brought even closer to the constriction by removing the Au layer right above the constriction, without affecting S_Φ. In this case (for a distance of 10 nm above the YBCO), ϕ_μ = 21 $n\Phi_0/\mu_B$ and $S_\mu^{1/2}$ = 62 $\mu_B/(\mathrm{Hz})^{1/2}$ at $B = 0$ and 110 $\mu_B/(\mathrm{Hz})^{1/2}$ at B = 1 T. The geometrical and electrical parameters for our device are summarized in Table 1.

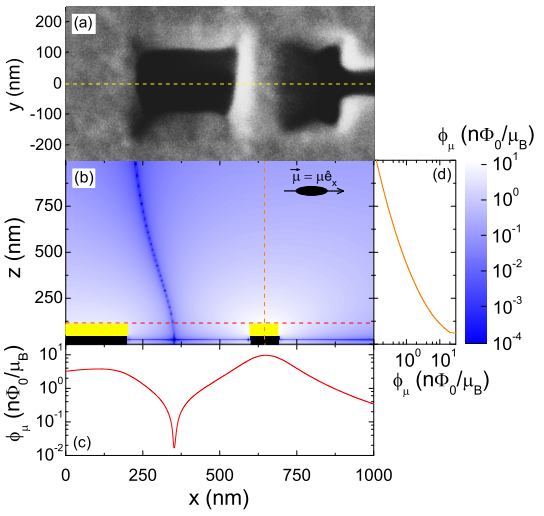

Figure 4. Calculated coupling factor ϕ_μ for the nanoSQUID. (a) SEM image showing SQUID hole and constriction in the (x,y) plane. The dashed line indicates the location of the (x,z) plane for which data are shown in (b); it also indicates the position of the linescan $\phi_\mu(x)$ shown in (c). (b) Contour plot of the coupling factor ϕ_μ *vs* position (x,z) of a magnetic moment pointing in the x-direction. Dashed lines indicate position of the linescans shown in (c) and (d). (c) Horizontal linescan $\phi_\mu(x)$ at a distance of 10 nm above the Au layer. (d) Vertical linescan $\phi_\mu(z)$ at the center of the constriction.

TABLE 1. Summary of Geometric and Electric NanoSQUID Parameters (As Defined in the Text)

d (nm)	l_c (nm)	l_j (nm)	w_c (nm)	w_j (nm)	β_L	L (pH)
50	300	400	90	130	0.65	36

I_0 (μA)	R (Ω)	I_0R (mV)	j_0 (mA/μm^2)	$S_\Phi^{1/2}$ ($n\Phi_0/(\mathrm{Hz})^{1/2}$)	ϕ_μ ($n\Phi_0/\mu_B$)	$S_\mu^{1/2}$ ($\mu_B/(\mathrm{Hz})^{1/2}$)
18.5	7.0	0.13	2.85	1300	21	62

CONCLUSIONS

In summary, we have demonstrated low-noise performance of a YBCO nanoSQUID in magnetic fields up to 1 T. At zero applied field, the white flux noise of the device at 7 kHz was 1.3 $\mu\Phi_0/(\mathrm{Hz})^{1/2}$, increasing only slightly to 2.3 $\mu\Phi_0/(\mathrm{Hz})^{1/2}$ at 1 T. For the spin sensitivity, assuming that a small particle is placed onto a constriction in the SQUID loop, directly on top of the YBCO film, we calculated values of 62 $\mu_B/(\mathrm{Hz})^{1/2}$ at $B = 0$ and 110 $\mu_B/(\mathrm{Hz})^{1/2}$ at B = 1 T.

The device investigated experimentally was not optimized yet in terms of its geometrical and electrical parameters. In particular, the thickness of the epitaxially grown YBCO films can be increased (to ~300 nm). This, in turn, would decrease the SQUID inductance by approximately a factor of 10, which will significantly reduce the flux noise. However, such an increase in thin film thickness will also reduce the coupling factor.

Hence, one has to carefully optimize all SQUID parameters by also taking into account technological constraints. Very recently, we performed such an optimization study, for YBCO nanoSQUIDs operated at 4.2 K and below, which predicts an optimum spin sensitivity of a few $\mu_B/(\mathrm{Hz})^{1/2}$. It remains to be shown whether or not such values can be achieved in high fields.

Furthermore, we note that miniaturized YBCO dc SQUIDs have been already used to investigate the magnetic properties of magnetic microcrystals at 0.12 T between 30 and 70 K.[42] Hence, due to their high T_c, YBCO nanoSQUIDs might also be useful for applications over a wide temperature range up to 70−80 K, such as for the investigation of the transition between the superparamagnetic and ferromagnetic state of magnetic nanoparticles. Optimization of the SQUID parameters for such a large temperature range—and according variation in the critical current of the grain boundary junctions and hence in the noise parameter Γ, the inductance parameter β_L and the Stewart−McCumber parameter β_C—will be more challenging than for operation at a few Kelvin and below. Still, such an approach may be rewarding because highly sensitive YBCO SQUIDs operating at 77 K have been demonstrated in the past.[46]

METHODS

Film Deposition. The films were deposited on 10 mm × 10 mm (1 mm thick) $SrTiO_3$ [001] bicrystal substrates. The substrates contain a single symmetric [001] tilt grain boundary with misorientation angle $\Theta = 24°$. After mounting the substrates by sliver paste on the sample holder, they were transferred to the ultrahigh vacuum (UHV) thin film deposition cluster tool (base pressure 10^{-9} mbar), equipped with a pulsed laser deposition (PLD) chamber and an electron beam evaporation (EBE) chamber. In the PLD chamber, 60 nm thick YBCO films were grown epitaxially by using a pulsed KrF excimer laser (wavelength 248 nm, pulse frequency 2 Hz), which is ablating material from a stochiometric YBCO target (purity 99.995%) with an energy density of ∼2 J/cm^2 of the laser spot on the target. During deposition at an oxygen pressure $p_{O_2} = 0.2$ mbar, the substrate was heated to a temperature T_s = 780 °C by a laser heating system. For the used 60 mm substrate-to-target distance, the PLD parameters yield a deposition rate of 9.8 nm/s. After deposition, the pressure was increased to p_{O_2} = 450 mbar; subsequently, T_s was reduced to 450 °C and kept there for 30 min before cooling the sample to room temperature. For the next deposition step, the sample was transferred in UHV to the EBE chamber, where a 60 nm thick Au film was deposited by electron beam evaporation (deposition rate ∼0.2 nm/s).

FIB Patterning. FIB patterning was performed in a FEI Dualbeam Strata 235, equipped with a Ga ion source. Parameters for FIB milling needed to be chosen carefully, as this patterning step can suppress superconductivity of YBCO. In the cutting scheme, which finally permitted the fabrication of nanoscaled Josephson junctions with no significant reduction of the critical current density j_c, Ga ion currents where adjusted to 30 pA at an acceleration voltage of 30 kV. Four rectangular patterns cut line-by-line (cleaning cross section cut), with cutting directions pointing away from the Josephson junctions, were placed at the grain boundary to form the final SQUID layout.

Measurements of Electric Transport Properties and Noise. The transport and noise measurements were performed at $T = 4.2$ K in an electrically shielded environment. We used a four-terminal configuration with filtered lines to measure IVCs, critical current $I_c(I_{mod})$, and $V(I_{mod})$. For transport measurements, the voltage V across the SQUID was amplified using a room temperature amplifier. All currents were applied by battery-powered current sources. In-plane magnetic fields up to $B = 7$ T could be applied by a split coil superconducting magnet. As magnetic fields that couple into the Josephson junctions suppress their critical current and hence the modulation amplitude of the SQUID, the SQUID loop needed to be aligned with high accuracy parallel to the magnetic field, and the in-plane field was aligned perpendicular to the grain boundary. To do so, the sample was mounted on two goniometers with perpendicular tilt axes (minimum step size 0.02 m°) and a rotator (minimum step size 0.5 m°). Alignment was done by monitoring and maximizing I_c at $B \sim 1$ T.

For noise measurements, the voltage drop across the nanoSQUID was preamplified by a dc SQUID amplifier[49] with 0.l nV/(Hz)$^{1/2}$ resolution and ∼30 kHz bandwidth. In this case, the SQUID was shunted by the input resistance $R_{inp} = 10\ \Omega$ of the SQUID amplifier. The thermal noise of the input resistance (at $T = 4.2$ K) limits the voltage resolution of the SQUID amplifier. To minimize stray fields, the SQUID amplifier was placed inside a Nb shield mounted inside the cryostat at a position of minimum magnetic field. Still, for $B \sim 1.5$ T (at the sample position), the SQUID amplifier trapped magnetic flux, preventing noise measurements at higher fields.

Conflict of Interest: The authors declare no competing financial interest.

Acknowledgment. We gratefully acknowledge S. Menzel for helping us with his expertise and with FIB facilities at IFW Dresden in the early stage of this project. J.N. and T.S acknowledge support by the Carl-Zeiss-Stiftung. This work was funded by the Nachwuchswissenschaftlerprogramm of the Universität Tübingen, by the Deutsche Forschungsgemeinschaft (DFG) *via* the SFB/TRR 21 and by the European Research Council *via* SOCATHES.

REFERENCES AND NOTES

1. Gatteschi, D.; Sessoli, R. Quantum Tunneling of Magnetization and Related Phenomena in Molecular Materials. *Angew. Chem., Int. Ed.* **2003**, *42*, 268–297.
2. Bogani, L.; Vindigni, A.; Sessoli, R.; Gatteschi, D. Single Chain Magnets: Where to from Here? *J. Mater. Chem.* **2008**, *18*, 4750–4758.
3. Fortágh, J.; Zimmermann, C. Toward Atom Chips. *Science* **2005**, *307*, 860–861.
4. Bushev, P.; Bothner, D.; Nagel, J.; Kemmler, M.; Konovalenko, K. B.; Loerincz, A.; Ilin, K.; Siegel, M.; Koelle, D.; Kleiner, R.; *et al.* Trapped Electron Coupled to Superconducting Devices. *Eur. Phys. J. D* **2011**, *63*, 9–16.
5. Rugar, D.; Budakian, R.; Mamin, H. J.; Chui, B. W. Single Spin Detection by Magnetic Resonance Force Microscopy. *Nature* **2004**, *430*, 329–332.
6. Maze, J. R.; Stanwix, P. L.; Hodges, J. S.; Hong, S.; Taylor, J. M.; Cappellaro, P.; Jiang, L.; Gurudev Dutt, M. V.; Togan, E.; Zibrov, A. S.; *et al.* Nanoscale Magnetic Sensing with an Individual Electronic Spin in Diamond. *Nature* **2008**, *455*, 644–647.
7. Balasubramanian, G.; Chan, I. Y.; Kolesov, R.; Al-Hmoud, M.; Tisler, J.; Shin, C.; Kim, C.; Wojcik, A.; Hemmer, P. R.; Krueger, A.; *et al.* Nanoscale Imaging Magnetometry with Diamond Spins under Ambient Conditions. *Nature* **2008**, *455*, 648–651.
8. Manassen, Y.; Hamers, R. J.; Demuth, J. E.; Castellano, A. J., Jr. Direct Observation of the Precession of Individual Paramagnetic Spins on Oxidized Silicon Surfaces. *Phys. Rev. Lett.* **1989**, *62*, 2531–2534.

9. Durkan, C.; Welland, M. E. Electronic Spin Detection in Molecules Using Scanning-Tunneling-Microscopy-Assisted Electron-Spin Resonance. *Appl. Phys. Lett.* **2002**, *80*, 458–460.
10. Theil Kuhn, L.; Geim, A. K.; Lok, J. G. S.; Hedegård, P.; Ylänen, K.; Jensen, J. B.; Johnson, E.; Lindelof, P. E. Magnetisation of Isolated Single Crystalline Fe-Nanoparticles Measured by a Ballistic Hall Micro-Magnetometer. *Eur. Phys. J. D* **2000**, *10*, 259–263.
11. Kazakova, O.; Panchal, V.; Gallop, J.; See, P.; Cox, D. C.; Spasova, M.; Cohen, L. F. Ultrasmall Particle Detection Using a Submircon Hall Sensor. *J. Appl. Phys.* **2010**, *107*, 09E708.
12. Voss, R. F.; Laibowitz, R. B.; Broers, A. N. Niobium Nanobridge dc SQUID. *Appl. Phys. Lett.* **1980**, *37*, 656–658.
13. Wernsdorfer, W. Classical and Quantum Magnetization Reversal Studied in Nanometersized Particles and Clusters. *Adv. Chem. Phys.* **2001**, *118*, 99–190.
14. Lam, S. K. H.; Tilbrook, D. L. Development of a Niobium Nanosuperconducting Quantum Interference Device for the Detection of Small Spin Populations. *Appl. Phys. Lett.* **2003**, *82*, 1078–1080.
15. Cleuziou, J.-P.; Wernsdorfer, W.; Bouchiat, V.; Ondarçuhu, T.; Monthioux, M. Carbon Nanotube Superconducting Quantum Interference Device. *Nat. Nanotechnol.* **2006**, *1*, 53–59.
16. Troeman, A. G. P.; Derking, H.; Borger, B.; Pleikies, J.; Veldhuis, D.; Hilgenkamp, H. NanoSQUIDs Based on Niobium Constrictions. *Nano Lett.* **2007**, *7*, 2152–2156.
17. Huber, M. E.; Koshnick, N. C.; Bluhm, H.; Archuleta, L. J.; Azua, T.; Björnsson, P. G.; Gardner, B. W.; Halloran, S. T.; Lucero, E. A.; Moler, K. A. Gradiometric Micro-SQUID Susceptometer for Scanning Measurements of Mesoscopic Samples. *Rev. Sci. Instrum.* **2008**, *79*, 053704.
18. Granata, C.; Esposito, E.; Vettoliere, A.; Petti, L.; Russo, M. An Integrated Superconductive Magnetic Nanosensor for High-Sensitivity Nanoscale Applications. *Nanotechnology* **2008**, *19*, 275501.
19. Wu, C. H.; Chou, Y. T.; Kuo, W. C.; Chen, J. H.; Wang, L. M.; Chen, J. C.; Chen, K. L.; Sou, U. C.; Yang, H. C.; Jeng, J. T. Fabrication and Characterization of High-T_c $YBa_2Cu_3O_{7-x}$ NanoSQUIDs Made by Focused Ion Beam Milling. *Nanotechnology* **2008**, *19*, 315304.
20. Koshnick, N. C.; Huber, M. E.; Bert, J. A.; Hicks, C. W.; Large, J.; Edwards, H.; Moler, K. A. A Terraced Scanning Superconducting Quantum Interference Device Susceptometer with Submicron Pickup Loops. *Appl. Phys. Lett.* **2008**, *93*, 243101.
21. Foley, C. P.; Hilgenkamp, H. Why NanoSQUIDs Are Important: An Introduction to the Focus Issue. *Supercond. Sci. Technol.* **2009**, *22*, 064001.
22. Vohralik, P. F.; Lam, S. K. H. NanoSQUID Detection of Magnetization from Ferritin Nanoparticles. *Supercond. Sci. Technol.* **2009**, *22*, 064007.
23. Bouchiat, V. Detection of Magnetic Moments Using a Nano-SQUID: Limits of Resolution and Sensitivity in Near-Field SQUID Magnetometry. *Supercond. Sci. Technol.* **2009**, *22*, 064002.
24. Faucher, M.; Jubert, P.-O.; Fruchart, O.; Wernsdorfer, W.; Bouchiat, V. Optimizing the Flux Coupling between a NanoSQUID and a Magnetic Particle Using Atomic Force Microscope Nanolithography. *Supercond. Sci. Technol.* **2009**, *22*, 064010.
25. Finkler, A.; Segev, Y.; Myasoedov, Y.; Rappaport, M. L.; Ne'eman, L.; Vasyukov, D.; Zeldov, E.; Huber, M. E.; Martin, J.; Yacoby, A. Self-Aligned Nanoscale SQUID on a Tip. *Nano Lett.* **2010**, *10*, 1046–1049.
26. Hao, L.; Aßmann, C.; Gallop, J. C.; Cox, D.; Ruede, F.; Kazakova, O.; Josephs-Franks, P.; Drung, D.; Schurig, T. Detection of Single Magnetic Nanobead with a Nano-Superconducting Quantum Interference Device. *Appl. Phys. Lett.* **2011**, *98*, 092504.
27. Lam, S. K. H.; Clem, J. R.; Yang, W. A Nanoscale SQUID Operating at High Magnetic Fields. *Nanotechnology* **2011**, *22*, 455501.
28. Nagel, J.; Kieler, O. F.; Weimann, T.; Wölbing, R.; Kohlmann, J.; Zorin, A. B.; Kleiner, R.; Koelle, D.; Kemmler, M. Superconducting Quantum Interference Devices with Submicron Nb/HfTi/Nb Junctions for Investigation of Small Magnetic Particles. *Appl. Phys. Lett.* **2011**, *99*, 032506.
29. Mandal, S.; Bautze, T.; Williams, O. A.; Naud, C.; Étienne Bustarret,; Omnès, F.; Rodière, P.; Meunier, T.; Bäuerle, C.; Saminadayar, L. The Diamond Superconducting Quantum Interference Device. *ACS Nano* **2011**, *5*, 7144–7148.
30. Russo, R.; Granata, C.; Esposito, E.; Peddis, D.; Cannas, C.; Vettoliere, A. Nanoparticle Magnetization Measurements by a High Sensitive Nano-Superconducting Quantum Interference Device. *Appl. Phys. Lett.* **2012**, *101*, 122601.
31. Van Harlingen, D. J.; Koch, R. H.; Clarke, J. Superconducting Quantum Interference Device with Very Low Magnetic Flux Noise Energy. *Appl. Phys. Lett.* **1982**, *41*, 197–199.
32. Gallop, J. SQUIDs: Some Limits to Measurement. *Supercond. Sci. Technol.* **2003**, *16*, 1575–1582.
33. Kleiner, R.; Koelle, D.; Ludwig, F.; Clarke, J. Superconducting Quantum Interference Devices: State-of-the-Art and Applications. *Proc. IEEE* **2004**, *92*, 1534–1548.
34. Chen, L.; Wernsdorfer, W.; Lampropoulos, C.; Christou, G.; Chiorescu, I. On-Chip SQUID Measurements in the Presence of High Magnetic Fields. *Nanotechnology* **2010**, *21*, 405504.
35. Wernsdorfer, W. From Micro- to Nano-SQUIDs: Applications to Nanomagnetism. *Supercond. Sci. Technol.* **2009**, *22*, 064013.
36. Drung, D.; Mück, M. In *The SQUD Handbook*; Clarke, J., Braginski, A. I., Eds.; Wiley-VCH: Weinheim, Germany, 2004; Vol. 1: Fundamentals and Technology of SQUIDs and SQUID Systems, Chapter 4, pp 127–170.
37. Hao, L.; Macfarlane, J. C.; Gallop, J. C.; Cox, D.; Beyer, J.; Drung, D.; Schurig, T. Measurement and Noise Performance of Nano-Superconducting-Quantum-Interference Devices Fabricated by Focused Ion Beam. *Appl. Phys. Lett.* **2008**, *92*, 192507.
38. Romans, E. J.; Rozhko, S.; Young, L.; Blois, A.; Hao, L.; Cox, D.; Gallop, J. C. Noise Performance of Niobium Nano-SQUIDs in Applied Magnetic Fields. *IEEE Trans. Appl. Supercond.* **2011**, *21*, 404–407.
39. Gross, R.; Alff, L.; Beck, A.; Froehlich, O.; Koelle, D.; Marx, A. Physics and Technology of High Temperature Superconducting Josephson Junctions. *IEEE Trans. Appl. Supercond.* **1997**, *7*, 2929–2935.
40. Hilgenkamp, H.; Mannhart, J. Grain Boundaries in High-T_c Superconductors. *Rev. Mod. Phys.* **2002**, *74*, 485.
41. Nagel, J.; Konovalenko, K. B.; Kemmler, M.; Turad, M.; Werner, R.; Kleisz, E.; Menzel, S.; Klingeler, R.; Büchner, B.; Kleiner, R.; *et al.* Resistively Shunted $YBa_2Cu_3O_7$ Grain Boundary Junctions and Low-Noise SQUIDs Patterned by a Focused Ion Beam down to 80 nm Linewidth. *Supercond. Sci. Technol.* **2011**, *24*, 015015.
42. Takeda, K.; Mori, H.; Yamaguchi, A.; Ishimoto, H.; Nakamura, T.; Kuriki, S.; Hozumi, T.; Ohkoshi, S. High Temperature Superconductor Micro-Superconducting-Quantum-Interference-Device Magnetometer for Magnetization Measurement of a Microscale Magnet. *Rev. Sci. Instrum.* **2008**, *79*, 033909.
43. Stewart, W. C. Current-Voltage Characteristics of Josephson Junctions. *Appl. Phys. Lett.* **1968**, *12*, 277.
44. McCumber, D. Effect of ac Impedance of dc Voltage-Current Characteristics of Josephson Junctions. *J. Appl. Phys.* **1968**, *39*, 3113.
45. Tesche, C. D.; Clarke, J. DC SQUID: Noise and Optimization. *J. Low Temp. Phys.* **1977**, *29*, 301–331.
46. Koelle, D.; Kleiner, R.; Ludwig, F.; Dantsker, E.; Clarke, J. High-Transition-Temperature Superconducting Quantum Interference Devices. *Rev. Mod. Phys.* **1999**, *71*, 631–686.
47. Chesca, B.; Kleiner, R.; Koelle, D. In *The SQUD Handbook*; Clarke, J., Braginski, A. I., Eds.; Wiley-VCH: Weinheim, Germany, 2004; Vol. 1: Fundamentals and Technology of SQUIDs and SQUID Systems, Chapter 2, pp 29–92.
48. Khapaev, M.; Kupriyanov, M.; Goldobin, E.; Siegel, M. Current Distribution Simulation for Superconducting Multi-Layered Structures. *Supercond. Sci. Technol.* **2003**, *16*, 24–27.
49. SQ100 LTS dc SQUID, PC-100 Single-Channel dc SQUID Electronics System, STAR Cryoelectronics, USA.